Xue et al. Nanoscale Research Letters (2017) 12:480
DOI 10.1186/s11671-017-2259-6

Nanoscale Research Letters

NANO EXPRESS Open Access

Facile Synthesis of Silver Nanowires with Different Aspect Ratios and Used as High-Performance Flexible Transparent Electrodes

Qingwen Xue[1], Weijing Yao[1], Jun Liu[1], Qingyong Tian[1], Li Liu[1], Mengxiao Li[1], Qiang Lu[1], Rui Peng[1] and Wei Wu[1,2*]

Abstract

Silver nanowires (Ag NWs) are the promising materials to fabricate flexible transparent electrodes, aiming to replace indium tin oxide (ITO) in the next generation of flexible electronics. Herein, a feasible polyvinylpyrrolidone (PVP)-mediated polyol synthesis of Ag NWs with different aspect ratios is demonstrated and high-quality Ag NWs transparent electrodes (NTEs) are fabricated without high-temperature thermal sintering. When employing the mixture of PVP with different average molecular weight as the capping agent, the diameters of Ag NWs can be tailored and Ag NWs with different aspect ratios varying from ca. 30 to ca. 1000 are obtained. Using these as-synthesized Ag NWs, the uniform Ag NWs films are fabricated by repeated spin coating. When the aspect ratios exceed 500, the optoelectronic performance of Ag NWs films improve remarkably and match up to those of ITO films. Moreover, an optimal Ag NTEs with low sheet resistance of 11.4 Ω/sq and a high parallel transmittance of 91.6% at 550 nm are achieved when the aspect ratios reach almost 1000. In addition, the sheet resistance of Ag NWs films does not show great variation after 400 cycles of bending test, suggesting an excellent flexibility. The proposed approach to fabricate highly flexible and high-performance Ag NTEs would be useful to the development of flexible devices.

Keywords: Ag NWs, Tailorable aspect ratios, Flexible transparent electrodes, Low-temperature welding

Background

Flexible transparent electrodes (FTEs) play an important role in the next generation of flexible electronics [1–4]. FTEs can be applied to many optoelectronic devices as conductive components, involving touch screens [5, 6], portable solar cells [7, 8], organic light-emitting diodes (OLEDs) [9–11], fuel cell electrode [12–17], sensors [18, 19], PM filter [20], transparent heaters [21, 22], and wearable electronics [23, 24]. The dominant transparent electrodes (TEs) used currently is indium tin oxide (ITO) owing to the low sheet resistance (<100 Ω/sq) and high transmittance (>80%). But its intrinsic brittleness limits the applications in flexible electronics. Moreover, it requires high temperature deposition process and is challenged by the scarcity of indium [25–27]. Therefore, several new conductive films with good flexibility and optical transparency, such as metal grids [2, 28, 29], carbon nanotubes (CNTs) [30–33], graphene [34–36], Ag NWs [5, 37–41], Cu NWs [42, 43], conductive polymers [44, 45], and hybrids of these [46–48], have been fabricated, striving to replace ITO. Among these candidates, Ag NWs films have been investigated extensively in both the scientific and industrial institutions, owing to the excellent electrical conductivity and high optical transparency. In addition, Ag NWs exhibit outstanding flexibility and stretchability, which is the one of the appealing advantage to fabricate stretchable transparent conductors than fragile ITO [49–51]. Moreover, the solution-processed Ag NWs

* Correspondence: weiwu@whu.edu.cn
[1]Laboratory of Printable Functional Nanomaterials and Printed Electronics, School of Printing and Packaging, Wuhan University, Wuhan 430072, People's Republic of China
[2]Shenzhen Research Institute of Wuhan University, Shenzhen 518057, People's Republic of China

films are more cost-effective than ITO. All of these properties make Ag NWs films become promising alternatives to ITO for the applications in flexible electronics.

However, several issues need to be addressed to commercialize Ag NWs films as FTEs. Firstly, Ag NWs with different aspect ratios need to be facilely synthesized in controlled manner because the alluring properties of Ag NWs films deeply rely on the dimensions of Ag NWs and a well-designed length and diameter are of very importance for different applications [52, 53]. Generally, polyol process is the most widely used method to prepare Ag NWs. Ran et al. [54] synthesized thin Ag NWs with aspect ratios larger than 1000 by using the mixed PVP with the average molecular weight of 58,000 and 1,300,000 as the capping agent. However, the influence of the aspect ratios on the optoelectronic performance of Ag NTEs was not carefully investigated in their work. Although Ding et al. [55] prepared Ag NWs with different diameters varying from 40 to 110 nm and fabricated Ag NTEs with a transmittance of 87% and a sheet resistance of ca.70 Ω/sq, many parameters need to be simultaneously adjusted to control the diameters of Ag NWs and the optoelectronic performance of the as-obtained Ag NTEs would not be satisfactory. Li et al. [56] synthesized thin Ag NWs with diameters of 20 nm through altering the concentration of bromide. And they have fabricated high-quality Ag NWs films with a transmittance of 99.1% at 130.0 Ω/sq. Ko et al. [57] developed a multistep growth method to synthesize very long Ag NWs over several hundred micrometers and the fabricated films demonstrated superior transmittance of 90% with sheet resistance of 19 Ω/sq. The optoelectronic performance of these Ag NWs films are comparable to or even better than those of ITO films. But the minimum aspect ratio of Ag NWs, which has the ability to fabricate TEs rivaling commercial ITO in terms of sheet resistance and transmittance, is still uncertain. Therefore, it is necessary to synthesize Ag NWs with various aspect ratios and study their influence on the optoelectronic performance of Ag NWs films.

Furthermore, the electronic conductivity of Ag NWs films is relatively poor, resulting from the high nanowire junction resistance [58]. In the polyol synthesis of Ag NWs, PVP, as the surfactant, adsorbs on the surface of Ag NWs, resulting in insulated contact between the wires in the random network [59, 60]. Consequently, different physical and chemical post-processes, involving thermal annealing [38, 39, 61, 62], mechanical press [63], nanosoldering with conductive polymers [64], plasmonic welding [65], laser nanowelding [66–68], and integration with other materials [60], have been explored to reduce the junction resistance. Among these post-treatments, thermal annealing at almost 200 °C is usually employed. It is incompatible with flexible plastic substrates which cannot withstand high temperature, and hence limits the applications of Ag NWs films in flexible optoelectronic devices.

Herein, a series of Ag NWs with different aspect ratios varying from ca. 30 to ca. 1000 are controllably synthesized and used to fabricate high conductive and transparent Ag NTEs. First, Ag NWs are prepared by facile PVP-mediated polyol process where the mixture of PVP with different average molecular weight can efficiently reduce the diameters. Subsequently, the as-synthesized Ag NWs with different aspect ratios are employed to fabricate Ag NWs films without high-temperature annealing, respectively. And the corresponding optoelectronic performance are comparative investigated. The best sheet resistance and parallel transmittance can achieve 11.4 Ω/sq and 91.6% when the aspect ratios reach almost 1000. Moreover, the sheet resistance of as-fabricated Ag NWs films is nearly constant after inner-bending and outer-bending tests.

Methods

Materials and Chemicals

Silver nitrate ($AgNO_3$, AR) and anhydrous ethanol (C_2H_5OH, AR) were purchased from Sinopharm Chemical Reagent Co., Ltd. Copper (II) chloride dehydrate ($CuCl_2{\cdot}2H_2O$, AR) and PVP (MW≈58,000, marked as PVP-58) were purchased from Shanghai Aladdin Reagents Co., Ltd. Ethylene glycol (EG, 98%) and PVP (MW≈10,000, 40,000 and 360,000, marked as PVP-10, PVP-40, and PVP-360, respectively) were purchased from Sigma-Aldrich. Deionized water (18.2 MΩ) was used in the whole experiments.

Synthesis of Ag NWs

Ag NWs with different aspect ratios are prepared by a facile one-pot PVP-mediated polyol process. Typically, 0.170 g of $AgNO_3$ is dissolved in 10 mL of EG under magnetic stirring. Then, 0.15 M of PVP-40 and 0.111 mM of $CuCl_2{\cdot}2H_2O$ mixed solution in 10 mL of EG is added dropwise to the above solution. Afterwards, the mixture is transferred into Teflon-lined stainless steel autoclave with a capacity of 50 mL and heated at 160 °C for 3 h. After cooling down to room temperature naturally, pure Ag NWs are obtained by centrifugation at a speed of 2500 rpm for 5 min and washed three times with ethanol and deionized water. Finally, the products are dispersed in ethanol for further characterization and application. Moreover, the concentration and average molecular weight of PVP are very important to control the morphology and size of products. Therefore, different types of PVP molecules are simultaneously used to regulate the diameters of Ag NWs in the polyol process. Detailed

experimental parameters are listed in Additional file 1: Table S1, nominated as S1–S13, respectively.

Fabrication of Ag NTEs

Polyethylene terephthalate (PET) with a thickness of 150 μm is cut to pieces with the dimension of 20 × 20 mm. Briefly, the as-prepared Ag NWs are dispersed in ethanol (6 mg/mL), and 50 μL of Ag NWs solution is spin coated at 2000 rpm for 30 s on PET substrate. Finally, the Ag NWs films are heated to 140 °C for 15 min without any additional post-process treatments. The aspect ratios of Ag NWs, rotation speed, concentration, and volume of Ag NWs solution are investigated to fabricate high-quality NTEs. Regarding to the repeated spin coating, each volume of Ag NWs solution is altered to 25 μL and the rotation speed is set to 2000 rpm. A time interval in each spin coating is needed to volatilize the ethanol. Other parameters are same as the aforementioned processes.

Characterization and Performance Test

Scanning electron microscopy (SEM) images are recorded using a cold field-emission SEM (Hitachi S-4800). The transmission electron microscopy (TEM) and the high-resolution TEM (HRTEM) images are obtained by using a JEOL JEM-2100F. The UV-vis absorption spectra of Ag NWs and the optical transmittance spectra of Ag NWs films are carried out on a Shimadzu UV-3600 spectrophotometer. The sheet resistance is measured at room temperature by using 4-point probe resistance tester (FP-001).

Results and Discussion

Generally, Ag NWs are synthesized by polyol process in which PVP is employed as capping agent to ensure the growth of one-dimensional Ag NWs [69, 70]. During the synthesis, many parameters such as reaction temperature, stirring speed, PVP concentration, PVP chain length, additive agents, and ratio of chemicals can affect the yield and morphology of synthesized Ag NWs. For example, an inappropriate reaction temperature less than 110 °C or higher than 180 °C allows more Ag atom to form Ag nanoparticles (NPs) rather than Ag NWs [70, 71]. The length of synthesized Ag NWs increase as slowing down the stirring speed [72, 73]. In this paper, we mainly investigate the concentration of PVP and their average molecular weight on the effect of morphology and size of Ag NWs. The corresponding morphology and size distribution of Ag NWs are demonstrated in Fig. 1 and Additional file 1: Figure S1. Firstly, the concentration of PVP is increased from 0.05 M (sample S1, Additional file 1: Figure S1a) to 0.15 M (sample S2, Fig. 1a). The corresponding morphology of products is changed from near-spherical Ag NPs to pure Ag NWs with an average diameter of 104.4 nm and length of 12.3 μm. The mixture of Ag NWs and Ag NPs are observed when the concentration of PVP is increased to 0.25 M (sample S3, Additional file 1: Figure S1b). By further increasing the concentration of PVP to

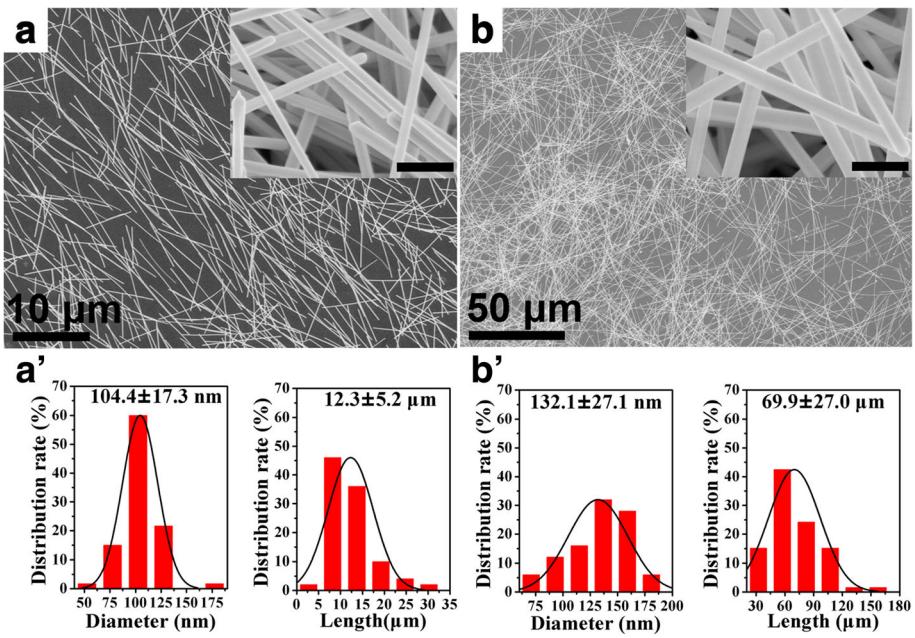

Fig. 1 **a**, **b** SEM images of as-synthesized Ag NWs with PVP-40 and PVP-360, respectively. Both the concentration of PVP are 0.15 M. **a' b'** Corresponding statistical distribution of diameter and length. (The *insets* in **a** and **b** are the corresponding SEM images with high magnification and all the *scale bars* are 500 nm)

0.55 M (sample S4, Additional file 1: Figure S1c), a large number of Ag NPs with different shapes (including near-sphere and triangular plate) are formed. The results indicate that a lower or higher concentration of PVP are not beneficial to produce pure Ag NWs, further resulting in the absence of Ag NWs. The formation of Ag NPs in the products upon changing the concentration of PVP can be attributed to the failure of anisotropic growth over the entire surface of multiply twinned nanoparticles (MTPs) [69, 74].

In addition, the influence of PVP with different molecular weight on the morphology and size of Ag NWs is also discussed. Only Ag NPs and aggregated nanorods are produced when using PVP-10 (sample S5, Additional file 1: Figure S1d). When employing separately PVP-58 (sample S6, Additional file 1: Figure S1e) and PVP-360 (sample S7, Fig. 1b), the corresponding morphology and size of products are changed from stubby Ag NWs (with average diameter of 235 nm and length of 6.7 μm) to high aspect ratio Ag NWs (with average diameter of 132.1 nm and length of 69.9 μm). According to the abovementioned results from samples S2, S5, S6, and S7, the average molecular weight of PVP not only plays a vital role in the morphology formation of Ag NWs but also has a significant influence on the diameter and length of Ag NWs products. The influence of PVP with different average molecular weight on the morphology and size of Ag NWs can be ascribed to three factors: (i) PVP as the capping agent prefers to adsorb on the side faces of MTPs [69]. The strong chemical adsorption promotes the growth of long Ag NWs [75]. (ii) The steric effect of PVP capping layer allows silver atoms to deposit on the side faces through the gap between adjacent PVP molecules, further resulting in the formation of thick Ag NWs [54]. (iii) The high viscosity of PVP with high average molecular weight in EG solution would slow down the growth rate, which are benefit to form MTPs [76, 77]. As a result, the low average molecular weight of PVP, like as PVP-10, would not efficiently adsorb on the (100) crystal faces to restrict the lateral growth. Meanwhile, the small steric effect and low viscosity would not prevent the aggregation of silver nanostructures. PVP with high molecular weight, like as PVP-360, possesses strong chemical adsorption on the side faces to produce long Ag NWs. But the large steric effect of PVP-360 would lead to the increase of diameter.

In order to obtain high aspect ratios of Ag NWs, the adsorption strength and steric effect should be reached to a state of balance in the PVP-mediated system. Therefore, the mixed PVP molecules at different molar ratios are employed as capping agent and the corresponding morphology and size distribution of Ag NWs are showed in Fig. 2 and Additional file 1: Figure S2. When mixing PVP-58 with PVP-40 at the molar ratio of 1:1, Ag NWs with average diameter of 47.5 nm and length of 16.1 μm are obtained. While the molar ratio of PVP-40 and PVP-58 is adjusted to 1:2 or 2:1, the diameter of Ag NWs is increased. In addition, the aspect ratios of Ag NWs dramatically enlarge when mixing PVP-40 with PVP-360 because the diameters are reduced significantly. When the molar ratio of PVP-40 and PVP-360 is 1:1, the aspect ratios reach almost 1000 and the diameters have a more uniform distribution as shown in Fig. 2e.

The influence of mixed PVP with different chain length on the diameters of Ag NWs could be interpreted briefly in Scheme 1a. The long-chained PVP molecules can retard the lateral growth of Ag NWs owing to the strong adsorption to the (100) facets. The large steric effect, resulting from the long chains, brings a relatively large distance between adjacent PVP molecules. Ag

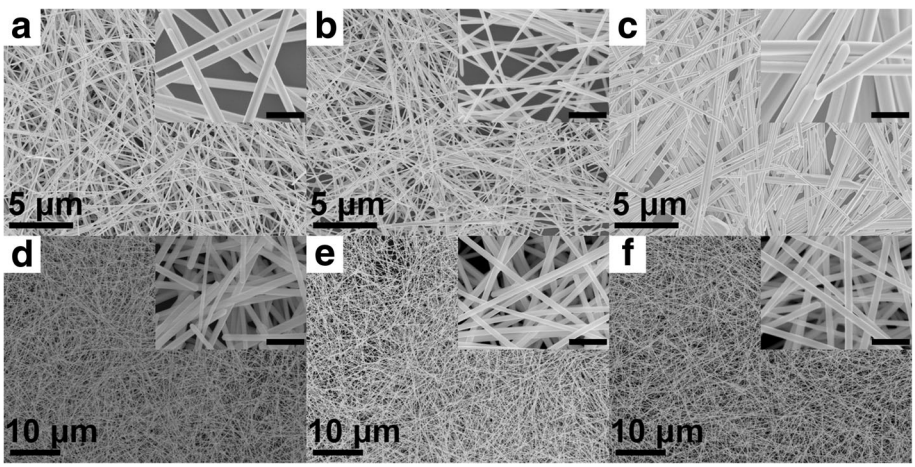

Fig. 2 SEM images of Ag NWs synthesized using different mixed PVP molecules. **a** PVP-40:PVP-58 = 2:1, **b** PVP-40:PVP-58 = 1:1, **c** PVP-40:PVP-58 = 1:2, **d** PVP-40:PVP-360 = 2:1, **e** PVP-40:PVP-360 = 1:1, **f** PVP-40:PVP-360 = 1:2, respectively. All the total concentration of PVP are 0.15 M, and different PVP molecules are mixed at molar ratio. (The *insets* in **a**–**f** are the corresponding SEM images with high magnification, and all the *scale bars* are 500 nm)

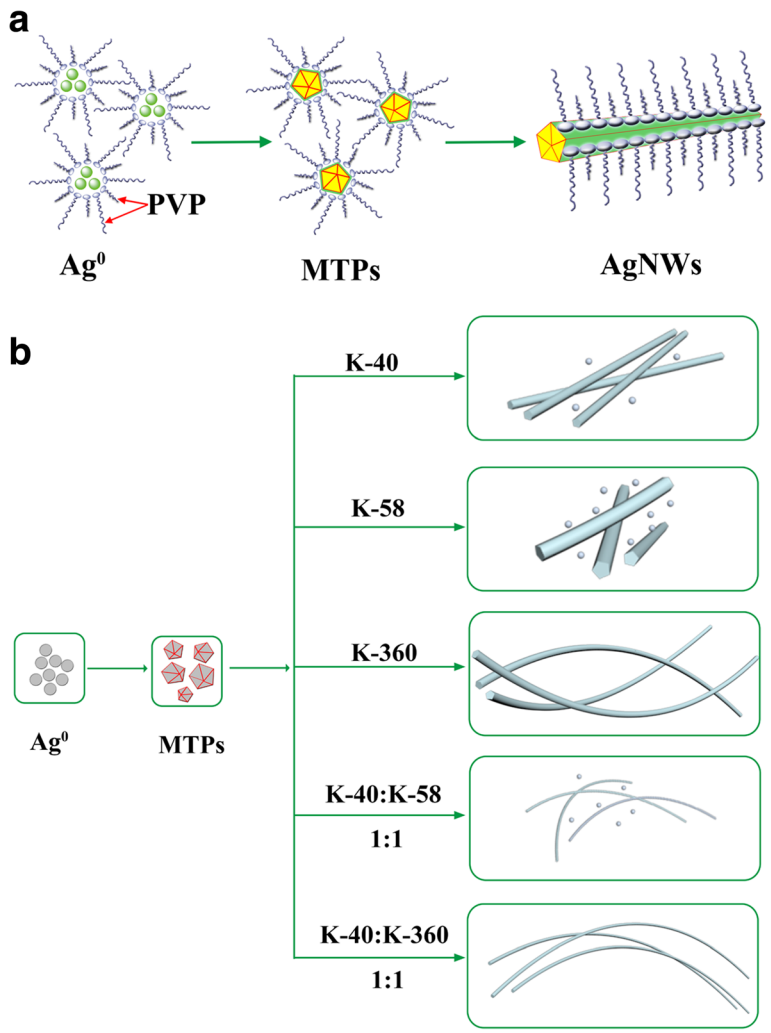

Scheme 1 **a** Schematic illustration of the growth mechanism of Ag NWs using mixed PVP with different chain length. **b** Different aspect ratio Ag NWs are obtained by the PVP-mediated polyol process

atoms can still deposit on the surface of Ag NWs by diffusion through the gap between adjacent PVP molecules, and thick Ag NWs are produced. When using the mixed PVP with different chain length, the short-chained PVP can fill the gap between long-chained PVP. Therefore, the (100) facets can be passivated more efficiently, leading to the formation of smaller Ag seeds and thinner Ag NWs [76]. As shown in Scheme 1b, Ag NWs with typical aspect ratios are obtained in our work. It could be conjectured that higher aspect ratio Ag NWs may be produced through this experimental route.

The microstructure and morphology of Ag NWs are characterized by TEM and demonstrated in Fig. 3a, b. The single nanowire is coated by the thin PVP layer with a thickness of ca. 2 nm. Figure 3c shows the HRTEM image of Ag NWs with a good crystalline structure. The HRTEM image clearly exhibits that the spaces between periodic fringes are 0.235 and 0.202 nm, in good correspondence with the crystal plane spaces for (111) and (200) planes of face-centered cubic (fcc) Ag. Meanwhile, Ag NWs grow along the [110] direction, as marked by the white arrow, and it is similar to the results in the earlier reports [70, 76].

As shown in Fig. 4, the UV-visible absorption spectra of as-prepared Ag NWs are different from that of the quasi-spherical Ag NPs. The spectra of Ag NWs appear double characteristic peaks. A shoulder peak located at around 350 nm could be ascribed to the plasmon resonance of bulk silver film [70, 78]. The second peak could be attributed to the transverse plasmon mode of Ag NWs, and the peak position is related to the dimensions of silver nanostructures [79]. While the peak at around 570 nm, resulting from the longitudinal plasmon resonance, is absent in the spectra because the aspect ratios of as-prepared Ag NWs are far more than 5 [70, 80]. In addition, as marked by the dashed green line, the second peak has a shift to red with the increase of diameters.

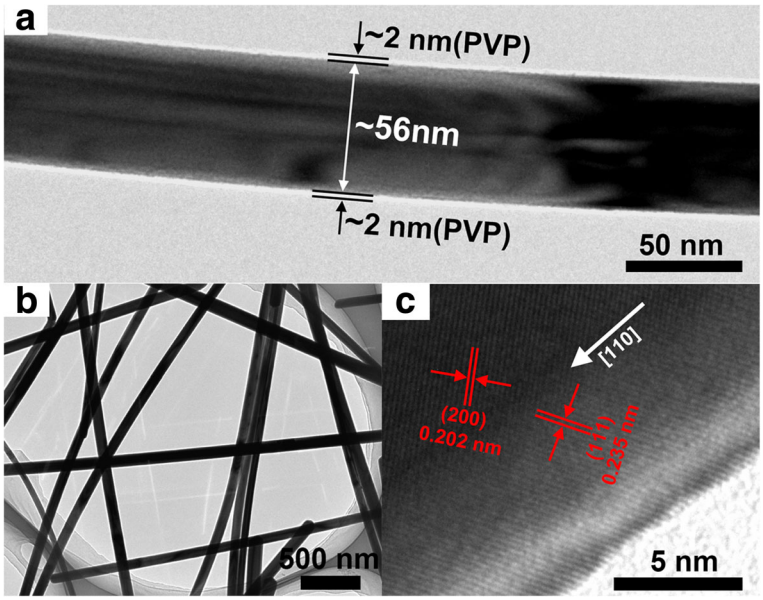

Fig. 3 TEM (**a**, **b**) and HRTEM (**c**) images of Ag NWs synthesized by mixing PVP-40 with PVP-360 (at a molar ratio of 1:1)

However, it is noteworthy that there is no obvious peak when the diameters of Ag NWs become larger. For Ag NWs from sample S6 (average diameter of 235 nm) and S10 (average diameter of 222.8 nm), the absorption intensity maximums locate at the wavelength of 408.5 and 406.5 nm, respectively. They are smaller than the peak wavelength of Ag NWs with smaller diameters from sample S7 (average diameter of 132.1 nm, the peak wavelength is 412 nm), indicating the detachment of red-shifted tendency of the right peak wavelength with larger diameters.

It is necessary to optimize the spin-coating process to fabricate high-quality Ag NWs films. As shown in Fig. 5a, it is observed that the sheet resistance increases as increasing the rotational speed because the number of Ag NWs clinging on the surface of PET decreases, resulting in the decline of conductivity. In addition, it is noteworthy that the sheet resistance significantly decreases to 19.6 Ω/sq when using the 8 mg/mL of Ag NWs solution. And it decreases almost fivefold compared with that of using 6 mg/mL, which could be attributed to the formation of more efficient conductive percolation routes in the Ag NWs network, whereas some macroscopic agglomerates of Ag NWs appears as the concentration increases to 8 mg/mL. Then, the repeated spin-coating process is carried out. As shown in Fig. 5b, both the transmittance and sheet resistance decrease as increasing the times of spin coating. More importantly, when the volume of Ag NWs solution is added from 50 to 75 μL, the sheet resistance dramatically decreases from 98.46 to 11.87 Ω/sq. As the volume further increases to 100 μL, the sheet resistance decreases to 10.42 Ω/sq with a transmittance of 80.95%. It indicates that the density of nanowires in the nanostructured transparent conducting networks may reach the tipping point where the transition from percolation behavior to bulk behavior occurs [81], when the volume is added to 75 μL. Moreover, to evaluate the performance of NTEs, the figure of merit (FOM) is calculated that correlates transmittance with sheet resistance. Generally, the transmittance (T_λ) and sheet resistance (R_s) of a thin metallic film satisfy the following Eq. (1):

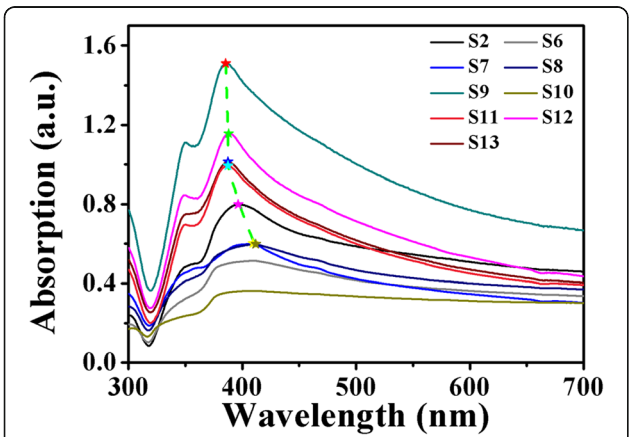

Fig. 4 UV-visible absorption spectra of as-prepared Ag NWs with different diameters

$$T_\lambda = \left(1 + \frac{188.5}{R_S}\frac{\sigma_{op}(\lambda)}{\sigma_{DC}}\right)^{-2} \quad (1)$$

$\sigma_{op}(\lambda)$ is the optical conductivity and σ_{DC} is the direct current conductivity of the film [37]. The value of $\sigma_{DC/}$

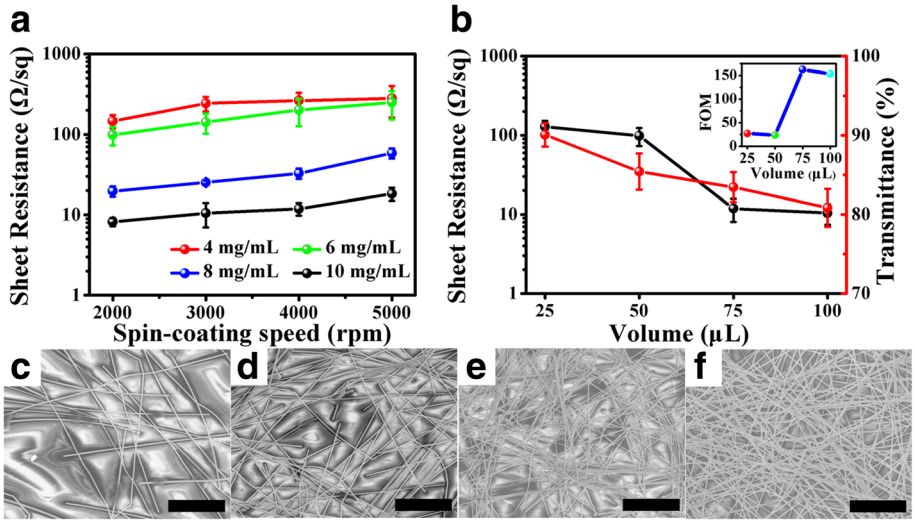

Fig. 5 **a** Sheet resistance of Ag NWs films vs the spin-coating speed at different concentration of Ag NWs. **b** Comparison of optoelectronic performance of Ag NTEs fabricated by different volume of Ag NWs solutions. The concentration of Ag NWs solution is 6 mg/mL, and the volume of each spin coating is 25 μL. The *inset* is the FOM values of Ag NWs films vs the volume of Ag NWs solution. **c**–**f** SEM images of Ag NWs films fabricated by different volumes of Ag NWs solutions, **c** 25 μL, **d** 50 μL, **e** 75 μL, **f** 100 μL, respectively. All the *scale bars* are 5 μm

$\sigma_{op}(\lambda)$ are employed as FOM. And a higher value of FOM means better optoelectronic performance. The inset in Fig. 5b exhibits the FOM values of NTEs fabricated by different volume of Ag NWs solutions. When the volume is added to 75 μL, the Ag NWs has the highest FOM value, increasing dramatically from 23.3 to 162.6. It denotes that the balance is achieved between low sheet resistance and high transmittance when implementing three times of spin coating. In addition, Fig. 5c–f shows the SEM images of Ag NWs films on PET with different densities, corresponding to the volume of Ag NWs solutions for 25, 50, 75, and 100 μl, respectively. From the images, it is obvious that the Ag NWs networks become ever denser and the distribution of Ag NWs is more uniform, as increasing the volume of Ag NWs solution. Therefore, the repeated spin-coating process is available to fabricate uniform Ag nanowire films with various transmittance and sheet resistance for different applications.

For application in NTEs, the nanowire junctions have a significant influence on the conductivity of random Ag NWs network [58]. In polyol process, the as-synthesized Ag NWs retain a residual insulated PVP layer, resulting in high resistance at junctions and the deterioration of conductivity. Lee et al. [59] reported that the repeated solvent washing can reduce the PVP layer from ca. 4 nm to 0.5 nm and allows for room-temperature welding of the overlapping Ag NWs. Similarly, we repeated to wash the as-synthesized Ag NWs for three times with ethyl alcohol to remove the PVP layer as much as possible. As the abovementioned results in Fig. 3a, thin PVP layer with a thickness of 2 nm is left. It can not only efficiently reduce the junction resistance but also ensure the good dispersion of Ag NWs in the solvent. On the other hand, for widthless sticks in two dimensions, the critical number density (N_c) of sticks to create a percolation network is given by Eq. (2):

$$N_c \times L^2 = 5.71 \tag{2}$$

L is the length of nanowires [52]. This equation implies that the number density of Ag NWs required for percolation network is inversely proportional to the square of length. Hence, long nanowires tend to build a sparse and effective percolation network with a low number density. It can not only increase the light transmission but also improve the conductivity through building long percolation routes with less nanowire junctions.

Figure 6a shows the comparison of optoelectronic performance of NTEs fabricated by Ag NWs with different aspect ratios. For samples S2 and S9, the enlargement of parallel transmittance could be attributed to the smaller diameters which reduced from 104.4 to 47.5 nm because nanowires with smaller diameters can scatter less light, leading to a further decrease in haze. As the aspect ratios exceed 500 (sample S7), Ag NWs films with a parallel transmittance of 81.8% (87.2%) and a sheet resistance of 7.4 Ω/sq (58.4 Ω/sq) are obtained. The optoelectronic performance are comparable to those of commercial ITO films (85%, 55 Ω/sq) [5]. Furthermore, when the aspect ratios reach almost 1000 (sample S12), Ag NWs films show superior transmittance (91.6–95.0%) and electronic conductivity (11.4–51.1 Ω/sq) than ITO films.

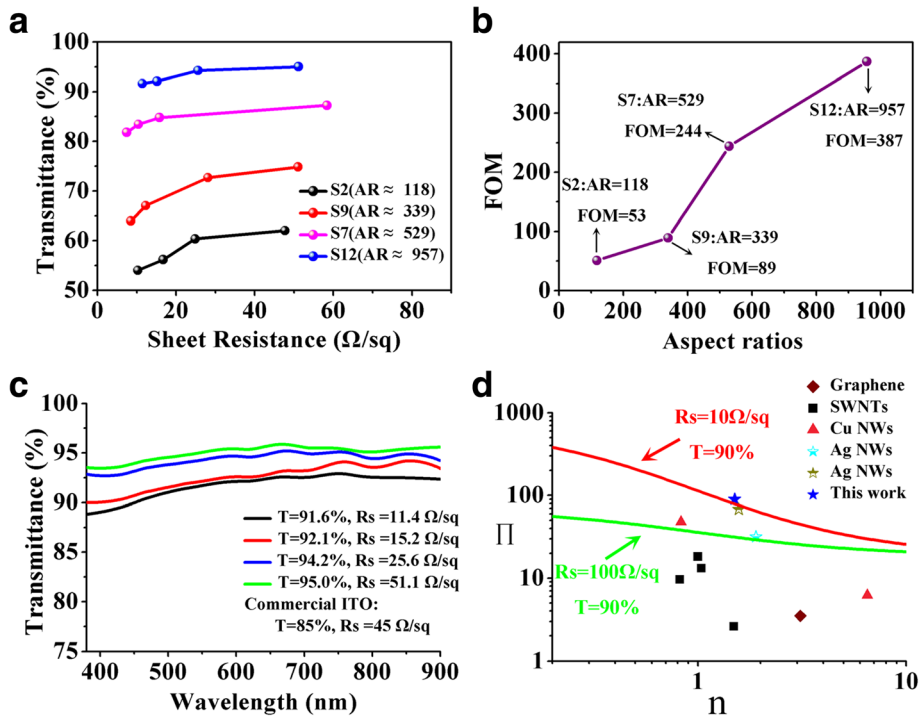

Fig. 6 **a** Comparison of optoelectronic performance of NTEs fabricated by Ag NWs with different aspect ratios (AR). **b** The best FOM values of Ag NWs films vs the AR of Ag NWs. **c** The optical transmittance spectra of Ag NWs films fabricated from sample S12. **d** Percolative figure of merit (*ΠΠ*), plotted against conductivity exponents (*n*). The *solid lines* are plotted at the given combinations of transmittance (*T*) and sheet resistance (R_s), as calculated from eq. (3). The plotted data of graphene, SWNTs, Cu NWs, Ag NWs are from recently published reports [37, 67, 81]. The *star symbol* represents the results of Ag NWs films fabricated using sample S12 from this work

They sufficiently meet the performance requirements of TEs in the application of solar cells or touch screens. Moreover, as shown in Fig. 6b, the biggest FOM value achieves 387, higher than many other reported values of various TEs [62, 73]. The excellent performance could be attributed to the long and thin Ag NWs. In addition, it is noteworthy that the FOM value dramatically increases from 89 to 224 when the aspect ratios enlarge from 339 (sample S9) to 529 (sample S7). The main reason is probably that the longer Ag NWs from sample S7 form a more effective percolation network with a smaller number of nanowires, leading to much more light transmission through the Ag NWs network. It indicates that the long Ag NWs strategy is a facile and effective way to obtain NTEs with promising optoelectronic performance, when the thin Ag NWs with a diameter less than 20 nm are not synthesized successfully [52, 67]. Figure 6c demonstrates optical transmittance spectra of Ag NWs films fabricated from sample S12. The spectra show a wide flat region from visible light to near infrared wavelength, which can improve the utilization range of light and is advantageous for display and solar cell applications, while the transmittance of ITO films displays dramatic fluctuation over the region of visible light [7].

To further evaluate the optoelectronic performance of Ag NWs networks, the percolative FOM, *ΠΠ*, was proposed in the Eq. (3) by De et al. [81]:

$$T = \left[1 + \frac{1}{\Pi}\left(\frac{Z_0}{R_S}\right)^{\frac{1}{n+1}}\right]^{-2} \quad (3)$$

Z_0 is the impedance of free space (377 Ω). T and R_s represent the transmittance and sheet resistance of Ag NWs films, respectively. High values of *ΠΠ* mean low sheet resistance and high transmittance. Percolative FOM (*ΠΠ*) and conductivity exponent (*n*) in this work are calculated to be 89.8 and 1.50 by using Eq. (3), respectively. The percolative FOM value is higher than other reported values of various TEs (shown in Fig. 6d). It could be attributed to two reasons: The thin PVP layer (ca. 2 nm) can effectively reduce the nanowire junction resistance. On the other hand, the long Ag NWs (ca. 71.0 μm) form long conductive routes in the percolation networks, resulting in the decrease of number of junctions. Interestingly, the value of *n* is a non-universal exponent which has been related to the presence of a distribution of nanowire junction resistance [82–84]. Lee et al. [67] used a laser nano-welding process to reduce the nanowire junction resistance, and the value of *n* is

calculated to be 1.57. The value is close to that in our work. It further suggests that the thin PVP layer and long Ag NWs are efficient to allow low-temperature welding of Ag NWs network.

Figure 7a exhibits optical photographs of the uniform Ag NWs film on PET. The film is highly transparent as the school badge in the background can be clearly seen through the film. Figure 7b, Additional file 1: Figure S3 and Additional file 2: Video S1 show that Ag NWs film on PET turn on the LED bulb when applying a low voltage. It indicates that the whole surface of Ag NWs film is highly conductive. In addition, The Ag NW film is very flexible as shown in Fig. 7c.

The mechanical stability of the fabricated Ag NTEs on PET substrate is evaluated by a bending test. As shown in Fig. 8, the bending test consists of 100 cycles of inner bending and 300 cycles of outer bending with a bending radio of 1.5 cm. No visible defects, such as cracking or tearing of the surface, are observed even after more than 400 cycles of bending test. And Ag NTEs exhibit a stable electronic performance with little change of sheet resistance. Its property to tolerate hundreds of mechanical bending test could be attributed to the flexibility of long Ag NWs and the benign adhesion to the substrate.

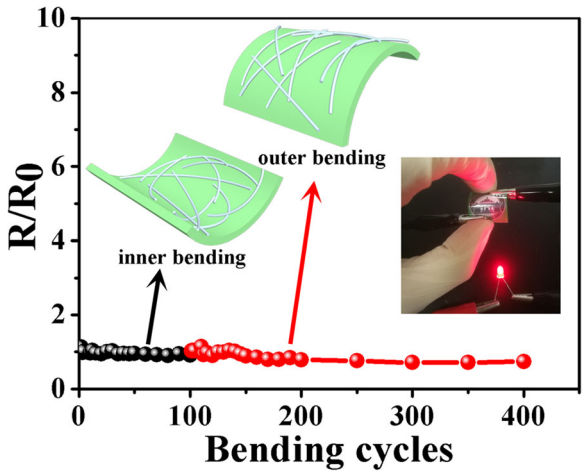

Fig. 8 The bending test, including inner bending and outer bending. Both the bending radios are 1.5 cm. The *inset* shows the bent Ag NTEs is still conductive over the whole surface. (R and R_0 represent the sheet resistance of films before and after bending test, respectively)

Conclusions

In summary, Ag NWs with different aspect ratios varying from ca. 30 to ca. 1000 are prepared via a facile PVP-mediated polyol process and are applied to the fabrication of high-performance Ag NTEs with low-temperature sintering. In the polyol process, the diameters of Ag NWs are strikingly reduced and the aspect ratios reach almost 1000 when employing mixed PVP as the capping agent. Additionally, when the aspect ratios exceed 500, the optoelectronic performance of Ag NWs films show good transmittance (81.8–87.2%) and electronic conductivity (7.4–58.4 Ω/sq), comparable to those of commercial ITO films (85%, 45 Ω/sq). Furthermore, high-performance Ag NTEs with a transmittance of 91.6% and a sheet resistance of 11.4 Ω/sq are obtained, as the aspect ratios exceed 1000. The long nanowires and thin PVP layer lead to less number of nanowire junctions and reduced junction resistance, respectively. It allows low-temperature sintering of Ag NWs network, which is advantageous for the applications in the flexible plastic substrates. Moreover, Ag NTEs show excellent flexibility against the bending test. We believe that the ability to synthesize Ag NWs with different aspect ratios and fabricate high-performance NTEs with low-temperature welding are very valuable to the development of flexible electronic devices.

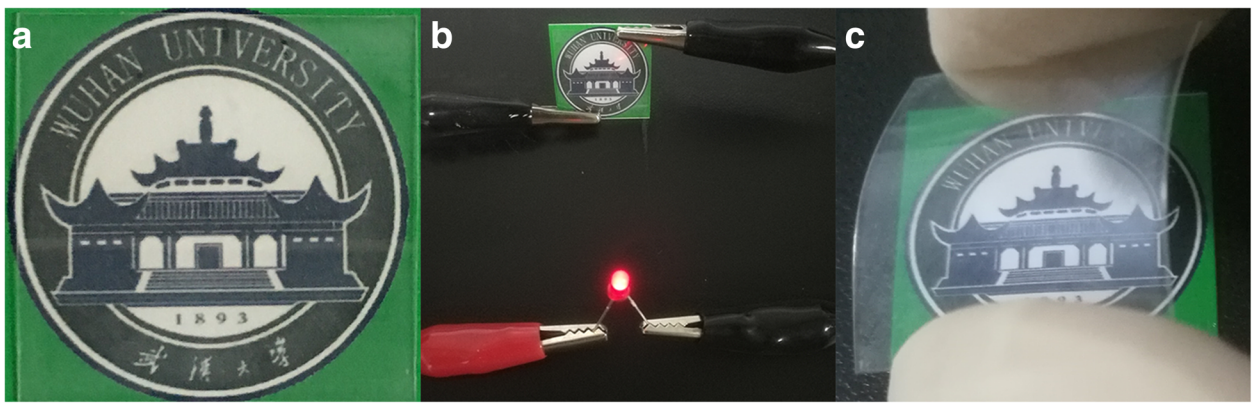

Fig. 7 **a** Optical image of as-fabricated Ag NWs films on PET. **b** Ag NWs film is connected in an electric circuit in which an LED is lit. **c** Optical image of the flexible Ag NWs film

Additional Files

Additional file 1: Table S1. Reaction parameters of Ag NWs with different concentrations of PVP and mixed PVP molecules at different mole ratios. Herein, silver nanoparticles and silver aggregated nanorods are abbreviated to Ag NPs and Ag ANRs, respectively. **Figure S1.** SEM images of Ag NWs under different reaction conditions: (a) 0.05 M PVP, (b) 0.25 M PVP, (c) 0.55 M PVP, (d) PVP-10, (e) PVP-58, respectively. (f) statistical size distribution of Ag NWs synthesized using PVP-58. **Figure S2.** Statistic sizes distribution of Ag NWs synthesized using different mixed PVP molecules. (a) PVP-40:PVP-58 = 2:1, (b) PVP-40:PVP-58 = 1:1, (c) PVP-40:PVP-58 = 1:2, (d) PVP-40:PVP-360 = 2:1, (e) PVP-40:PVP-360 = 1:1, (f) PVP-40:PVP-360 = 1:2, respectively. **Figure S3.** Ag NWs film is connected in an electric circuit, being applied a low voltage. (DOCX 2653 kb)

Additional file 2: The video of Ag NWs flexible transparent electrodes. (AVI 9706 kb)

Acknowledgements
This work was supported by the NSFC (51471121), Basic Research Plan Program of Shenzhen City (JCYJ20160517104459444, JCYJ20170303170426117), Natural Science Foundation of Jiangsu Province (BK20160383), and Wuhan University.

Authors' Contributions
QWX completed all the experiments and wrote the manuscript. WJY, JL, QYT, LL, MXL, QL, and RP assisted with the manuscript preparation. WW conceived the study, revised the manuscript, and supervised the work. All authors read and approved the final manuscript.

Competing Interests
The authors declare that they have no competing interests.

Publisher's Note

Received: 28 June 2017 Accepted: 31 July 2017
Published online: 07 August 2017

References
1. Liu Z, Xu J, Chen D, Shen G (2015) Flexible electronics based on inorganic nanowires. Chem Soc Rev 44(1):161–192
2. Khan A, Lee S, Jang T, Xiong Z, Zhang C, Tang J, Guo LJ, Li WD (2016) High-performance flexible transparent electrode with an embedded metal mesh fabricated by cost-effective solution process. Small 12(22):3021–3030
3. Liu JW, Wang JL, Wang ZH, Huang WR, Yu SH (2014) Manipulating nanowire assembly for flexible transparent electrodes. Angew Chem Int Ed 53(49):13477–13482
4. Ye S, Rathmell AR, Chen Z, Stewart IE, Wiley BJ (2014) Metal nanowire networks: the next generation of transparent conductors. Adv Mater 26(39):6670–6687
5. Jia Y, Chen C, Jia D, Li S, Ji S, Ye C (2016) Silver nanowire transparent conductive films with high uniformity fabricated via a dynamic heating method. ACS Appl Mater Interfaces 8(15):9865–9871
6. Kim D-J, Shin H-I, Ko E-H, Kim K-H, Kim T-W, Kim H-K (2016) Roll-to-roll slot-die coating of 400 mm wide, flexible, transparent Ag nanowire films for flexible touch screen panels. Sci Rep 6:34322
7. Jin Y, Li L, Cheng Y, Kong L, Pei Q, Xiao F (2015) Cohesively enhanced conductivity and adhesion of flexible silver nanowire networks by biocompatible polymer sol-gel transition. Adv Funct Mater 25(10):1581–1587
8. Kaltenbrunner M, White MS, Głowacki ED, Sekitani T, Someya T, Sariciftci NS, Bauer S (2012) Ultrathin and lightweight organic solar cells with high flexibility. Nat Commun 3:770
9. Liang J, Li L, Niu X, Yu Z, Pei Q (2013) Elastomeric polymer light-emitting devices and displays. Nat Photon 7(10):817–824
10. Liang J, Li L, Tong K, Ren Z, Hu W, Niu X, Chen Y, Pei Q (2014) Silver nanowire percolation network soldered with graphene oxide at room temperature and its application for fully stretchable polymer light-emitting diodes. ACS Nano 8(2):1590–1600
11. Lee J, A K, Won P, Ka Y, Hwang H, Moon H, Kwon Y, Hong S, Kim C, Lee C, Ko SH (2017) A dual-scale metal nanowire network transparent conductor for highly efficient and flexible organic light emitting diodes. Nano 9(5): 1978–1985
12. Chang I, Lee J, Lee Y, Lee YH, Ko SH, Cha SW (2017) Thermally stable Ag@ ZrO_2 core-shell via atomic layer deposition. Mater Lett 188:372–374
13. Chang I, Park T, Lee J, Lee HB, Ji S, Lee MH, Ko SH, Cha SW (2014) Performance enhancement in bendable fuel cell using highly conductive Ag nanowires. Int J Hydrog Energy 39(14):7422–7427
14. Chang I, Park T, Lee J, Lee HB, Ko SH, Cha SW (2016) Flexible fuel cell using stiffness-controlled endplate. Int J Hydrog Energy 41(14):6013–6019
15. Chang I, Park T, Lee J, Lee MH, Ko SH, Cha SW (2013) Bendable polymer electrolyte fuel cell using highly flexible Ag nanowire percolation network current collectors. J Mater Chem A 1(30):8541–8546
16. Park T, Chang I, Jung JH, Lee HB, Ko SH, O'Hayre R, Yoo SJ, Cha SW (2017) Effect of assembly pressure on the performance of a bendable polymer electrolyte fuel cell based on a silver nanowire current collector. Energy 134:412–419
17. Park T, Chang I, Lee HB, Ko SH, Cha SW (2017) Performance variation of bendable polymer electrolyte fuel cell based on Ag nanowire current collector under mixed bending and twisting load. Int J Hydrog Energy 42(3):1884–1890
18. Hong S, Yeo J, Lee J, Lee H, Lee P, Lee SS, Ko SH (2015) Selective laser direct patterning of silver nanowire percolation network transparent conductor for capacitive touch panel. J Nanosci Nanotech 15(3):2317–2323
19. Kim KK, Hong S, Cho HM, Lee J, Suh YD, Ham J, Ko SH (2015) Highly sensitive and stretchable multidimensional strain sensor with prestrained anisotropic metal nanowire percolation networks. Nano Lett 15(8):5240–5247
20. Jeong S, Cho H, Han S, Won P, Lee H, Hong S, Yeo J, Kwon J, Ko SH (2017) High efficiency, transparent, reusable, and active PM2.5 filters by hierarchical Ag nanowire percolation network. Nano Lett 17(7):4339–4346
21. Suh YD, Hong S, Lee J, Lee H, Jung S, Kwon J, Moon H, Won P, Shin J, Yeo J (2016) Random nanocrack, assisted metal nanowire-bundled network fabrication for a highly flexible and transparent conductor. RSC Adv 6(62): 57434–57440
22. Suh YD, Jung J, Lee H, Yeo J, Hong S, Lee P, Lee D, Ko SH (2017) Nanowire reinforced nanoparticle nanocomposite for highly flexible transparent electrodes: borrowing ideas from macrocomposites in steel-wire reinforced concrete. J Mater Chem C 5(4):791–798
23. Hong S, Lee H, Lee J, Kwon J, Han S, Suh YD, Cho H, Shin J, Yeo J, Ko SH (2015) Highly stretchable and transparent metal nanowire heater for wearable electronics applications. Adv Mater 27(32):4744–4751
24. Hwang B-U, Lee J-H, Trung TQ, Roh E, Kim D-I, Kim S-W, Lee N-E (2015) Transparent stretchable self-powered patchable sensor platform with ultrasensitive recognition of human activities. ACS Nano 9(9):8801–8810
25. De S, Coleman JN (2011) The effects of percolation in nanostructured transparent conductors. MRS Bull 36(10):774–781
26. Kim H, Horwitz J, Kushto G, Kafafi Z, Chrisey D (2001) Indium tin oxide thin films grown on flexible plastic substrates by pulsed-laser deposition for organic light-emitting diodes. Appl Phys Lett 79(3):284–286
27. Tian H, Xie D, Yang Y, Ren T-L, Wang Y-F, Zhou C-J, Peng P-G, Wang L-G, Liu L-T (2011) Transparent, flexible, ultrathin sound source devices using indium tin oxide films. Appl Phys Lett 99(4):043503
28. Van De Groep J, Spinelli P, Polman A (2012) Transparent conducting silver nanowire networks. Nano Lett 12(6):3138–3144
29. Sciacca B, van de Groep J, Polman A, Garnett EC (2016) Solution-grown silver nanowire ordered arrays as transparent electrodes. Adv Mater 28(5):905–909
30. Saran N, Parikh K, Suh D-S, Muñoz E, Kolla H, Manohar SK (2004) Fabrication and characterization of thin films of single-walled carbon nanotube bundles on flexible plastic substrates. J Am Chem Soc 126(14):4462–4463
31. Kang SJ, Kocabas C, Ozel T, Shim M, Pimparkar N, Alam MA, Rotkin SV, Rogers JA (2007) High-performance electronics using dense, perfectly aligned arrays of single-walled carbon nanotubes. Nat Nanotechnol 2(4): 230–236
32. Rowell MW, Topinka MA, McGehee MD, Prall H-J, Dennler G, Sariciftci NS, Hu L, Gruner G (2006) Organic solar cells with carbon nanotube network electrodes. Appl Phys Lett 88(23):233506
33. Wu W (2017) Inorganic nanomaterials for printed electronics: a review. Nano 9(22):7342–7372

34. El-Kady MF, Strong V, Dubin S, Kaner RB (2012) Laser scribing of high-performance and flexible graphene-based electrochemical capacitors. Science 335(6074):1326–1330
35. Bae S, Kim H, Lee Y, Xu X, Park J-S, Zheng Y, Balakrishnan J, Lei T, Kim HR, Song YI (2010) Roll-to-roll production of 30-inch graphene films for transparent electrodes. Nat Nanotechnol 5(8):574–578
36. Chen Z, Ren W, Gao L, Liu B, Pei S, Cheng H-M (2011) Three-dimensional flexible and conductive interconnected graphene networks grown by chemical vapour deposition. Nat Mater 10(6):424–428
37. De S, Higgins TM, Lyons PE, Doherty EM, Nirmalraj PN, Blau WJ, Boland JJ, Coleman JN (2009) Silver nanowire networks as flexible, transparent, conducting films: extremely high DC to optical conductivity ratios. ACS Nano 3(7):1767–1774
38. Scardaci V, Coull R, Lyons PE, Rickard D, Coleman JN (2011) Spray deposition of highly transparent, low-resistance networks of silver nanowires over large areas. Small 7(18):2621–2628
39. Lee J-Y, Connor ST, Cui Y, Peumans P (2008) Solution-processed metal nanowire mesh transparent electrodes. Nano Lett 8(2):689–692
40. Bari B, Lee J, Jang T, Won P, Ko SH, Alamgir K, Arshad M, Guo LJ (2016) Simple hydrothermal synthesis of very-long and thin silver nanowires and their application in high quality transparent electrodes. J Mater Chem A 4(29):11365–11371
41. Moon H, Won P, Lee J, Ko SH (2016) Low-haze, annealing-free, very long Ag nanowire synthesis and its application in a flexible transparent touch panel. Nanotechnology 27(29):295201
42. Han S, Hong S, Ham J, Yeo J, Lee J, Kang B, Lee P, Kwon J, Lee SS, Yang MY (2014) Fast plasmonic laser nanowelding for a Cu-nanowire percolation network for flexible transparent conductors and stretchable electronics. Adv Mater 26(33):5808–5814
43. Han S, Hong S, Yeo J, Kim D, Kang B, Yang MY, Ko SH (2015) Nanorecycling: monolithic integration of copper and copper oxide nanowire network electrode through selective reversible photothermochemical reduction. Adv Mater 27(41):6397–6403
44. Kim N, Kang H, Lee JH, Kee S, Lee SH, Lee K (2015) Highly conductive all-plastic electrodes fabricated using a novel chemically controlled transfer-printing method. Adv Mater 27(14):2317–2323
45. Hofmann AI, Smaal WT, Mumtaz M, Katsigiannopoulos D, Brochon C, Schütze F, Hild OR, Cloutet E, Hadziioannou G (2015) An alternative anionic polyelectrolyte for aqueous PEDOT dispersions: toward printable transparent electrodes. Angew Chem Int Ed 127(29):8626–8630
46. Hsiao S-T, Tien H-W, Liao W-H, Wang Y-S, Li S-M, MMa C-C, Yu Y-H, Chuang W-P (2014) A highly electrically conductive graphene-silver nanowire hybrid nanomaterial for transparent conductive films. J Mater Chem C 2(35):7284–7291
47. Zilberberg K, Gasse F, Pagui R, Polywka A, Behrendt A, Trost S, Heiderhoff R, Görrn P, Riedl T (2014) Highly robust indium-free transparent conductive electrodes based on composites of silver nanowires and conductive metal oxides. Adv Funct Mater 24(12):1671–1678
48. Deng B, Hsu P-C, Chen G, Chandrashekar B, Liao L, Ayitimuda Z, Wu J, Guo Y, Lin L, Zhou Y (2015) Roll-to-roll encapsulation of metal nanowires between graphene and plastic substrate for high-performance flexible transparent electrodes. Nano Lett 15(6):4206–4213
49. Lee H, Hong S, Lee J, Suh YD, Kwon J, Moon H, Kim H, Yeo J, Ko SH (2016) Highly stretchable and transparent supercapacitor by Ag-Au core-shell nanowire network with high electrochemical stability. ACS Appl Mater Interfaces 8(24):15449–15458
50. Lee P, Ham J, Lee J, Hong S, Han S, Suh YD, Lee SE, Yeo J, Lee SS, Lee D (2014) Highly stretchable or transparent conductor fabrication by a hierarchical multiscale hybrid nanocomposite. Adv Funct Mater 24(36): 5671–5678
51. Moon H, Lee H, Kwon J, Suh YD, Kim DK, Ha I, Yeo J, Hong S, Ko SH (2017) Ag/Au/polypyrrole core-shell nanowire network for transparent, stretchable and flexible supercapacitor in wearable energy devices. Sci Rep 7:41981
52. Bergin SM, Chen Y-H, Rathmell AR, Charbonneau P, Li Z-Y, Wiley BJ (2012) The effect of nanowire length and diameter on the properties of transparent, conducting nanowire films. Nano 4(6):1996–2004
53. Sorel S, Lyons PE, De S, Dickerson JC, Coleman JN (2012) The dependence of the optoelectrical properties of silver nanowire networks on nanowire length and diameter. Nanotechnology 23(18):185201
54. Ran Y, He W, Wang K, Ji S, Ye C (2014) A one-step route to Ag nanowires with a diameter below 40 nm and an aspect ratio above 1000. Chem Commun 50(94):14877–14880
55. Ding H, Zhang Y, Yang G, Zhang S, Yu L, Zhang P (2016) Large scale preparation of silver nanowires with different diameters by a one-pot method and their application in transparent conducting films. RSC Adv 6(10):8096–8102
56. Li B, Ye S, Stewart IE, Alvarez S, Wiley BJ (2015) Synthesis and purification of silver nanowires to make conducting films with a transmittance of 99%. Nano Lett 15(10):6722–6726
57. Lee JH, Lee P, Lee D, Lee SS, Ko SH (2012) Large-scale synthesis and characterization of very long silver nanowires via successive multistep growth. Cryst Growth Des 12(11):5598–5605
58. Bellew AT, Manning HG, Gomes da Rocha C, Ferreira MS, Boland JJ (2015) Resistance of single Ag nanowire junctions and their role in the conductivity of nanowire networks. ACS Nano 9(11):11422–11429
59. Lee J, Lee I, Kim TS, Lee JY (2013) Efficient welding of silver nanowire networks without post-processing. Small 9(17):2887–2894
60. Xiong W, Liu H, Chen Y, Zheng M, Zhao Y, Kong X, Wang Y, Zhang X, Kong X, Wang P (2016) Highly conductive, air-stable silver nanowire@longel composite films toward flexible transparent electrodes. Adv Mater 28(33): 7167–7172
61. Madaria AR, Kumar A, Ishikawa FN, Zhou C (2010) Uniform, highly conductive, and patterned transparent films of a percolating silver nanowire network on rigid and flexible substrates using a dry transfer technique. Nano Res 3(8):564–573
62. Madaria AR, Kumar A, Zhou C (2011) Large scale, highly conductive and patterned transparent films of silver nanowires on arbitrary substrates and their application in touch screens. Nanotechnology 22(24):245201
63. Hu L, Kim HS, Lee J-Y, Peumans P, Cui Y (2010) Scalable coating and properties of transparent, flexible, silver nanowire electrodes. ACS Nano 4(5):2955–2963
64. Lee J, Lee P, Lee HB, Hong S, Lee I, Yeo J, Lee SS, Kim TS, Lee D, Ko SH (2013) Room-temperature nanosoldering of a very long metal nanowire network by conducting-polymer-assisted joining for a flexible touch-panel application. Adv Funct Mater 23(34):4171–4176
65. Garnett EC, Cai W, Cha JJ, Mahmood F, Connor ST, Christoforo MG, Cui Y, McGehee MD, Brongersma ML (2012) Self-limited plasmonic welding of silver nanowire junctions. Nat Mater 11(3):241–249
66. Hong S, Lee H, Yeo J, Ko SH (2016) Digital selective laser methods for nanomaterials: from synthesis to processing. Nano Today 11(5):547–564
67. Lee J, Lee P, Lee H, Lee D, Lee SS, Ko SH (2012) Very long Ag nanowire synthesis and its application in a highly transparent, conductive and flexible metal electrode touch panel. Nano 4(20):6408–6414
68. Lee P, Lee J, Lee H, Yeo J, Hong S, Nam KH, Lee D, Lee SS, Ko SH (2012) Highly stretchable and highly conductive metal electrode by very long metal nanowire percolation network. Adv Mater 24(25):3326–3332
69. Sun Y, Mayers B, Herricks T, Xia Y (2003) Polyol synthesis of uniform silver nanowires: a plausible growth mechanism and the supporting evidence. Nano Lett 3(7):955–960
70. Sun Y, Gates B, Mayers B, Xia Y (2002) Crystalline silver nanowires by soft solution processing. Nano Lett 2(2):165–168
71. Sun Y, Xia Y (2002) Large-scale synthesis of uniform silver nanowires through a soft, self-seeding. Polyol Process Adv Mater 14(11):833–837
72. Araki T, Jiu J, Nogi M, Koga H, Nagao S, Sugahara T, Suganuma K (2014) Low haze transparent electrodes and highly conducting air dried films with ultra-long silver nanowires synthesized by one-step polyol method. Nano Res 7(2):236–245
73. Jiu J, Araki T, Wang J, Nogi M, Sugahara T, Nagao S, Koga H, Suganuma K, Nakazawa E, Hara M (2014) Facile synthesis of very-long silver nanowires for transparent electrodes. J Mater Chem A 2(18):6326–6330
74. Wiley B, Sun Y, Xia Y (2007) Synthesis of silver nanostructures with controlled shapes and properties. Acc Chem Res 40(10):1067–1076
75. Zhu J-J, Kan C-X, Wan J-G, Han M, Wang G-H (2011) High-yield synthesis of uniform Ag nanowires with high aspect ratios by introducing the long-chain PVP in an improved polyol process. J Nanomater 2011:982547
76. da Silva RR, Yang M, Choi S-I, Chi M, Luo M, Zhang C, Li Z-Y, Camargo PH, Ribeiro SJL, Xia Y (2016) Facile synthesis of sub-20 nm silver nanowires through a bromide-mediated polyol method. ACS Nano 10(8):7892–7900
77. Wang Y, Zheng Y, Huang CZ, Xia Y (2013) Synthesis of Ag nanocubes 18-32 nm in edge length: the effects of polyol on reduction kinetics, size control, and reproducibility. J Am Chem Soc 135(5):1941–1951

78. Kelly KL, Coronado E, Zhao LL, Schatz GC (2003) The optical properties of metal nanoparticles: the influence of size, shape, and dielectric environment. J Phys Chem B 107(3):668–677
79. Jain PK, Lee KS, El-Sayed IH, El-Sayed MA (2006) Calculated absorption and scattering properties of gold nanoparticles of different size, shape, and composition: applications in biological imaging and biomedicine. J Phys Chem B 110(14):7238–7248
80. Dickson RM, Lyon LA (2000) Unidirectional plasmon propagation in metallic nanowires. J Phys Chem B 104(26):6095–6098
81. De S, King PJ, Lyons PE, Khan U, Coleman JN (2010) Size effects and the problem with percolation in nanostructured transparent conductors. ACS Nano 4(12):7064–7072
82. Balberg I (1998) Limits on the continuum-percolation transport exponents. Phys Rev B 57(21):13351–13354
83. Grimaldi C, Balberg I (2006) Tunneling and nonuniversality in continuum percolation systems. Phys Rev Lett 96(6):066602
84. Johner N, Grimaldi C, Balberg I, Ryser P (2008) Transport exponent in a three-dimensional continuum tunneling-percolation model. Phys Rev B 77(17):174204